Ducted Turbine Blade Optimization Using Numerical Simulation

Michael Shives and Curran Crawford
Department of Mechanical Engineering, University of Victoria
Victoria, British Columbia, Canada

ABSTRACT

This paper presents a combined blade element (BE), computational fluid dynamics (CFD) method for performance analysis and optimization of ducted turbines. The model is similar to standard blade element momentum theory, except that CFD replaces the momentum equation for determining the induction factors. This eliminates many assumptions used in applying the typical blade element momentum (BEM) theory to a turbine and provides much richer flow information. It is also required for ducted turbines, since there is no fundamental momentum theory model that includes the impact of the duct on the flow field. The simulations use an axi-symmetric domain, which is computationally efficient since only a thin wedge of the entire geometry needs to be represented. A simple algorithm was developed to determine the optimum rotor loading and tip speed ratio for a given duct geometry within a user-defined level of granularity. This paper also demonstrates that for certain ducts, a non-uniform loading over the disk can improve overall performance by limiting flow separation within the duct.

KEY WORDS: Diffuser augmented turbine, tidal turbine, blade element, computational fluid dynamics.

INTRODUCTION

Diffuser augmentation of wind turbines has been studied for decades by academics and companies such as Vortec (NZ) but with no commercially successful designs. This is thought to be due in part to the immense loading on the duct in storm conditions. With an emerging potential for tidal power generation, there is renewed interest in diffuser augmented turbines since tidal flows are less subject to extreme velocities. For example, Ireland's OpenHydro has conducted tests with a high-solidity ducted turbine in the Bay of Fundy. Alstom (France) is developing a ducted turbine based on a design by Clean Current (Canada) also to be tested in the Bay of Fundy in 2012. Lunar energy (Scotland) and several other companies are also developing similar ducted designs.

Diffusers augment the mass flow through a turbine of a given area while accelerating the flow at the rotor, allowing the turbine power coefficient to exceed the well known Betz limit for an idealized open rotor. Diffuser augmentation was noted in the 1950s by Lilley and Rainbird (1956), who estimated that a power enhancement of 65% or more, compared to an open-flow (non-ducted) turbine, could reasonably be achieved. Later on, Foreman, Gilbert and Oman (1978) identified a 90% power enhancement over the non-ducted case from experimental results. Presently however, diffuser enhancement cannot be fully described by analytical models such as those by Lawn (2003) or Jamieson (2008, 2009) due to the requirement for empirical parameters which have not yet been adequately identified through experiments or simulations. This precludes using standard blade profile design tools based on blade element momentum (BEM) theory as published in many texts such as Burton *et al* (2001). Additionally, complex flow behaviour such as flow separation have a large influence on ducted turbine performance and can presently be modeled only using computational fluid dynamics (CFD). Note that pure potential flow codes would not be applicable due to their inability to predict flow separation, which is vital to ducted turbine performance.

The present research aims to develop a computationally efficient and straightforward CFD method to predict performance and optimize the hydrodynamic design of ducted turbines. The ultimate goal is a strategy to optimize the duct and blade profiles simultaneously. However, at present a method for blade design for a given duct has been developed and applied. The methodology relies on aspects of blade element theory and computational fluid dynamics. It is similar to the blade element momentum theory, except that CFD is used to predict the induction factors instead of momentum theory. A simple algorithm has been written to determine (within a chosen level of granularity) the optimum thrust coefficient C_T, tip speed ratio λ and a non-uniformity factor C_{nu} which defines a linear relationship in axial force with radius in the actuator disk. The rationale in using a non-uniform loading is to reduce flow separation in the duct by increasing the velocity at the outer radius of the turbine. The CFD simulations use an axi-symmetric assumption which reduces the computational domain drastically compared to a full 3D simulation. Blade profiles are calculated using the resulting flow field and determined blade-element forces.

The actuator disk approach neglects discrete blade effects (e.g. tip-loss). To address this, work is ongoing to develop and validate an actuator line method to quantify the importance of these effects for ducted turbines. The contribution of this research is to provide an efficient blade optimization methodology for ducted turbine design. The present method is fast enough for design work on a typical PC.

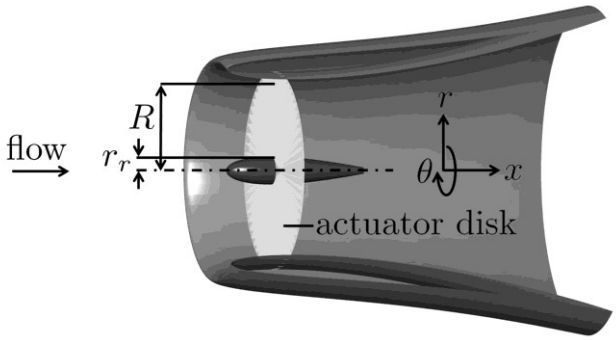

Fig. 1: Duct and actuator disk

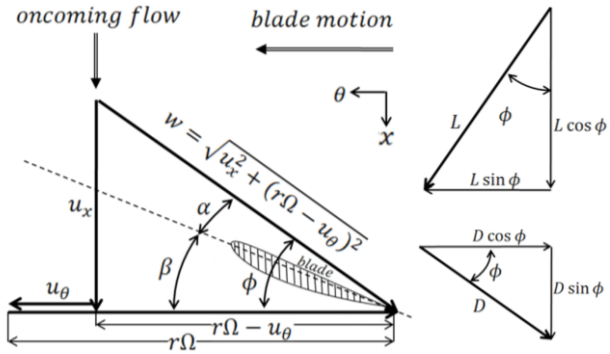

Fig. 2: Blade flow angles and forces

MODEL FRAMEWORK

The model uses an actuator disk representation of the turbine. The disk is implemented in the simulation as a sub-domain (Fig. 1) in which a momentum source term is specified. The momentum source is a force per unit volume, and consists of axial and tangential components. This allows the blade forces to be modeled without explicitly representing the blade geometry, reducing the computational domain significantly. In the model, C_T, λ, C_{nu} and the blade lift to drag ratio (l/d) are defined as input parameters. It is necessary to determine the axial and tangential force distributions within the actuator disk, which are derived in the next two sections. Once the forces are known, the rotor power can be calculated as a product of the torque and rotational speed Ω. Finally, the blade geometry can be calculated from the flow results and input parameters.

Axial Force

Assuming a uniform distribution, the axial force per unit volume $f_{x,uni}$ applied by the actuator disk is determined by the thrust coefficient according to eq. 1. Note that the actuator disk has a finite and constant thickness of t_d. This is a requirement of the chosen implementation method since a subdomain must occupy a volume in space.

$$f_x = f_{x,uni} = \frac{C_T \rho u_0^2}{2t_d} \tag{1}$$

If the axial force varies linearly with radius r, it can be shown that for an actuator disk with a root radius r_r and outer radius R, a C_T equal to the uniformly loaded case will give eq. 2. Here, C_{nu} is a ratio of the loading at $r = 0$ to the uniform loading. Thus, $C_{nu} > 1$ gives higher loading at the root than at the tip.

$$f_x = f_{x,uni}\left(C_{nu} + \frac{3(R^2 - r_r^2)}{2(R^3 - r_r^3)}(1 - C_{nu})r\right) \tag{2}$$

Tangential Force

This section derives a ratio between the axial and tangential blade forces. The formulation presented here specifies the tangential force without *a priori* knowledge of the chord and twist distribution. This allows the optimum blade geometry to emerge from the simulation.

It is possible to use a similar actuator disk model only considering the axial momentum. However such an approach does not represent the true physics of a turbine which generates power from the blade torque, which results from the tangential force. Also, a purely axial approach cannot be taken here because the angular velocity is required to calculate the blade twist and chord distributions. A purely axial approach would not account for the effects of blade drag or wake swirl.

To describe the relationship between axial and tangential force, it is useful to observe a diagram of the relevant flow velocities and angles from the perspective of a turbine blade cross section (Fig. 2). The turbine blade generates lift l perpendicular to the resultant velocity w, and drag d parallel to w. The lift and drag are transformed into the (x,θ) frame by rotating through the inflow angle ϕ, as shown in Fig. 2.

The tangential and axial forces on the blade are expressed by eqs. 3 and 4. For a given airfoil cross section the lift and drag vary with angle of attack α, and there is a certain value of α which maximizes the lift to drag ratio l/d. Using the lift to drag ratio allows the drag term d to be replaced with a fraction of the lift. The optimum blade design is such that the local angle of attack at all radial locations will be the one that maximizes the lift to drag ratio.

$$f_\theta = l \sin\phi - d\cos\phi \tag{3}$$

$$f_x = l \cos\phi - d\cos\phi \tag{4}$$

If a certain airfoil has been selected, and lift and drag polar data are available, the maximum l/d will be known. If multiple airfoil sections are to be used, then l/d can be defined as a function of r with no negative influence on the model performance.

The *sin* and *cos* terms can be defined as in eq. 5. It is then possible to define the ratio of tangential to axial force as a function of flow velocities, radial position and blade angular velocity as in eq. 6, which is valid at any radial position. Note that many equations in this paper use the inverse of the lift to drag ratio (i.e. d/l) for cleaner notation.

$$\sin\phi = \frac{u_x}{w} \qquad \cos\phi = \frac{r\Omega - u_\theta}{w} \tag{5}$$

$$\frac{f_\theta}{f_x} = \frac{u_x - \frac{d}{l}(r\Omega - u_\theta)}{(r\Omega - u_\theta) + \frac{d}{l}u_x} \tag{6}$$

Using eq. 6 it is possible to define the tangential force at any radial location along the blade as a function of the specified local axial force, blade angular speed, and the computed local velocity.

Blade Properties

This section describes how the blade chord and twist distributions are found once the CFD simulations are complete. The chord is found by relating the lift force acting on N blades at a radial position r to the simulated actuator disk force at that same radial location. In the actuator disk, the total lift force acting on an annulus of radius r and thickness dr is given by;

$$l_{disk} = \frac{-wf_x(2\pi r)d_r t_d}{r\Omega - u_\theta + \frac{d}{l}u_x} \tag{7}$$

For a set of N turbine blades, the total lift acting on that same annulus can be found from the airfoil lift coefficient using;

$$l_{blades} = \frac{1}{2}\rho w^2 c_l N c dr \tag{8}$$

Then, equating eqs. 7 and 8; solving for the chord c gives;

$$c = \frac{-f_x t_d 2\pi r}{N c_l \frac{1}{2}\rho w\left(r\Omega - u_\theta + \frac{d}{l}u_x\right)} \tag{9}$$

Using definitions for non-dimensional radius $\mu = r/R$, local speed ratio $\lambda_r = r\Omega/u_0$, induction factors $a = 1-u_x/u_0$ and $a' = -u_\theta/r\Omega$ and the definition for f_x (eq. 2) a non-dimensional relationship for the chord (eq. 10) can be defined. The induction factors can be found directly from the simulation, and eq. 10 can be used to find the chord distribution for the optimum c_l (corresponding to $l/d_{\max}$) and N.

$$\frac{c}{R} = \frac{C_T\left[C_{nu} + \frac{3}{2}\left(\frac{1-\mu_r^2}{1-\mu_r^3}\right)(1-C_{nu})\mu\right]2\pi\mu}{N c_l\sqrt{(1-a)^2+\lambda_r^2(1+a')^2}\left[\lambda_r(1+a') + \frac{d}{l}(1-a)\right]} \tag{10}$$

The blade twist distribution is more straightforward to find. Once the simulation is complete, the inflow angle ϕ is found using eq. 11. For a given optimum angle of attack α, known from airfoil data, the twist angle β (as shown in Fig. 2) is given by eq. 12.

$$\phi = \arctan\left(\frac{u_x}{r\Omega - u_\theta}\right) \tag{11}$$

$$\beta = \phi - \alpha \tag{12}$$

Power and Thrust

This section provides formulas for the total power coefficient C_P, as well as local power and thrust coefficients ($C_{P,local}$, $C_{T,local}$). The total power is calculated as the volume integral of the product of tangential force f_θ, radius r and rotational speed Ω, normalized by $\frac{1}{2}\rho u_0^3 A_{disk}$.

$$C_P = \frac{\int_{\mathcal{V}} f_\theta r\Omega d\mathcal{V}}{\frac{1}{2}\rho u_0^3 A_{disk}} \tag{13}$$

In contrast, the power coefficient calculated from a purely axial momentum approach would be given by eq. 14. Note that this formulation would neglect blade drag, which is included in the present approach in the relationship between f_θ and f_x.

$$C_P = \frac{\int_{\mathcal{V}} u_x f_x d\mathcal{V}}{\frac{1}{2}\rho u_0^3 A_{disk}} \tag{14}$$

The local thrust coefficient is defined in eq. 15 as the total thrust on an annulus of radius r and thickness dr, normalized by $\frac{1}{2}\rho u_0^2 A_{annulus}$. Then the local power coefficient is defined in eq. 16 as the power generated in the annulus, normalized by $\frac{1}{2}\rho u_0^3 A_{annulus}$. The local power is a product of the total tangential force on the annulus, the angular speed Ω and radius r.

$$C_{T,local} = C_T\left[C_{nu} + \frac{3}{2}\left\{\frac{1-\mu_r^2}{1-\mu_r^3}\right\}(1-C_{nu})\mu\right] \tag{15}$$

$$C_{P,local} = C_{T,local}\left[\frac{(1-a) - \frac{d}{l}\lambda_r(1+a')}{\lambda_r(1+a') + \frac{d}{l}(1-a)}\right]\lambda_r \tag{16}$$

Duct Geometry

A single duct geometry was considered for this paper. The duct was created by modifying a NACA 0015 airfoil using a similar methodology to that presented by Hansen, Sørensen and Flay (2000). The airfoil was first scaled in thickness by a factor $kt = 0.45$. A camber was then applied by rotating the geometry about the origin through a linearly varying angle (0° at the leading edge to 8.08° at the trailing edge). Finally the airfoil was translated by $\Delta r = 0.28$ to control the throat area. The modified airfoil geometry is shown in Fig. 3. A crude hub was also included by modifying the NACA 0015 airfoil. The thickness was altered such that the maximum cross sectional area of the hub was 2% of the duct throat area. The hub length was set to 40% of the duct length, and the hub maximum radius occurs at the duct throat location.

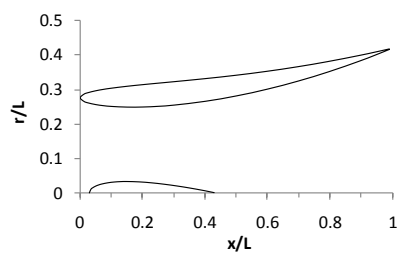

Fig. 3: Duct and hub profiles

CFD IMPLEMENTATION

Simulations were carried out using ANSYS CFX, following a similar methodology as Hansen, Sørensen and Flay (2000). The meshing strategy and simulation parameters were the same as in previous work by Shives and Crawford (2010a, 2010b). This paper progressed from the previous work by incorporating swirl effects, implementing non-uniform loading and developing the method to specify the chord and twist distribution of the blade.

The mesh was a 6° slice of the entire flow domain. Periodic boundary conditions were enforced to simulate the entire 360° domain. This mesh was created by sweeping a 2D structured surface mesh through a 6° rotation in two elements. In theory, this type of axi-symmetric simulation is two-dimensional, and only requires one element in the azimuthal direction, however CFX uses a 3D solver which requires at least two elements to apply periodic boundary conditions. Turbulence was modeled using the $k\omega$-SST option due to its known applicability to predicting boundary layer separation in adverse pressure gradients. No model for the transition from laminar to turbulent flow was used as the flow is assumed to be turbulent along the entire duct surface.

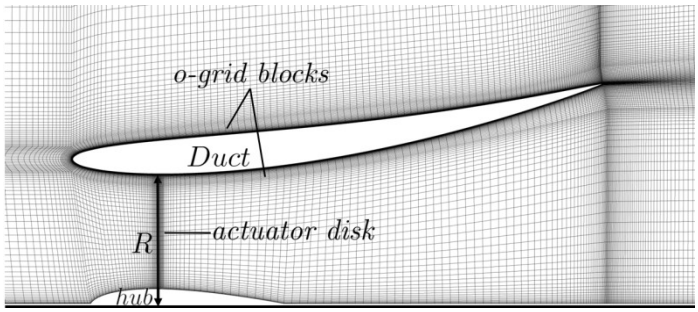

Fig. 4: Mesh near the duct

The domain distances were normalized based on the duct length $L = 1$ m. The inlet was *5L* upstream of the duct leading edge and enforced a uniform velocity of 1 m/s. The outlet was *10L* downstream of the trailing edge and enforced $p = p_0$. As in the work of Hansen, Sørensen and Flay (2000), an inner radial boundary employing a free-slip condition was used to avoid a singularity in azimuthal velocity at the centerline. This boundary was located such that the inner core area was 0.1% of the duct throat area. The outer radial boundary was located at $r = 5L$ and was treated using the opening for entrainment option, which approximates an infinite domain. The actuator disk was located at the duct throat.

Grid Convergence

To ensure minimal grid resolution error, the effect of grid refinement on the power coefficient was studied. Adequate resolution of the boundary layer along the duct was considered crucial. The grid refinement study was conducted following guidelines by Celik *et al* (2008). Three meshes of progressively greater refinement were developed. The meshing strategy was a C-grid approach as shown in Fig. 4. The number of nodes in each 2D mesh were, N1=169164, N2=85256, N3=44451.

The power coefficient was chosen as the target variable. Simulations were run with the inlet turbulence intensity set to 1% and 20%. The gird convergence study results are summarized in Table 1, which shows that even with the coarse mesh, the expected discretization error was less than 2%. The medium mesh was used for all further simulations to ensure reasonable grid convergence when applying this meshing strategy to different duct geometries, and because it gave reasonable simulation runtimes of 15 to 60 minutes using 4 parallel processes on a recent i7core PC.

Table 1: Grid convergence study results

	$\phi = C_P$	
Parameter	$I_{inlet} = 1\%$	$I_{inlet} = 20\%$
ϕ_1	0.8141	0.8532
ϕ_2	0.8137	0.8531
ϕ_3	0.8126	0.8533
ϕ_{ext}	0.8539	0.8533
GCI_{fine}	0.18%	0.03%
GCI_{med}	0.24%	0.04%
GCI_{coarse}	0.41%	0.01%

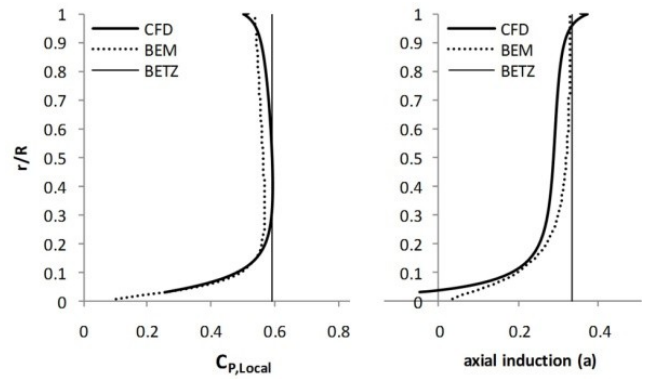

Fig. 5: Comparison of local power coefficient (left) and axial induction factor (right) for BEM and AD-RANS for an open flow turbine.

VALIDITY OF THE METHODOLOGY

It is necessary to validate the current simulation methodology using experimental data to ensure that the model behaves similarly to real ducted turbines. At this time such validation has not been completed because suitable experimental data are not publicly available for a ducted turbine.

For open flow turbines, on the other hand, the actuator disk with computational fluid dynamics (AD-CFD) approach has been successfully applied by a number of researchers and is recognized as a valid modeling tool. In a review paper on the state of the art of wind turbine aerodynamics, Hansen *et al* (2006) identified fifteen papers using the AD-CFD approach. Since then, many researchers have used the approach to study a wide variety of phenomena. Examples include; Sun, Chick and Bryden (2008) who studied the interaction of free-surface deformation and tidal power extraction, Harrison et al (2010) who modeled tidal turbine wake recovery and Singh and Dinavahi (2011) who performed shape optimization of a ducted propulsion system. The AD-CFD approach produces results which typically agree very well with experimental data. Mikkelsen (2003) for example, showed a very good agreement between CFD results and experimental data for the Nordtank NTK 500/41 wind turbine with LM 19.1m blades. More recently, Réthoré, Sørensen and Zahle (2010) showed that the AD-CFD flowfield agrees very well with the exact analytical solution provided by Conway (1995).

In this study, the AD-RANS approach was compared to the industry standard blade element momentum theory for an open flow turbine. The blade element momentum formulations presented in Burton *et al.* (2001), which include the effect on the axial flow of pressure reduction in the wake due to swirl velocity, were used. For this comparison, the actuator disk was uniformly loaded at $C_T = 8/9$ and $l/d = 100$ was assumed. The resulting axial induction and local power coefficient are plotted in Fig. 5. There is a good general agreement between the two approaches. It is evident that the CFD model predicts a lower axial induction, and higher local power coefficient than the BEM approach. It is thought that these discrepancies are due to the transfer of momentum between annular sections (from the outer edge of the disk and inward radially) which is captured in the CFD model, but inherently neglected in the BEM model.

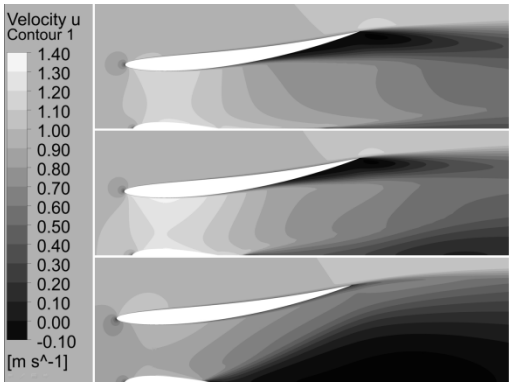

Fig. 6: Contour of axial velocity, uniform case with $C_T = 0.8$ (top), and non-uniform cases with $C_T = 0.80$, $C_{nu} = 1.3$ (middle) and $C_T = 0.85$, $C_{nu} = 1.3$ (bottom).

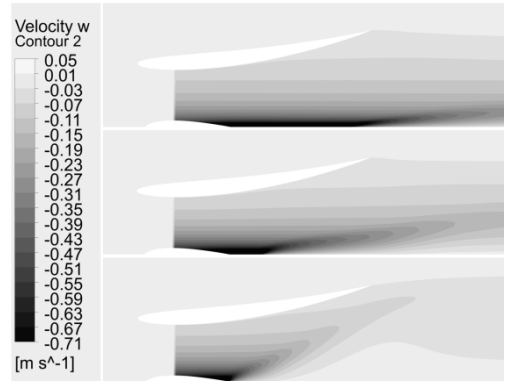

Fig. 7: Contour of swirl velocity, uniform case with $C_T = 0.8$ (top), and non-uniform cases with $C_T = 0.80$, $C_{nu} = 1.3$ (middle) and $C_T = 0.85$, $C_{nu} = 1.3$ (bottom)

OPTIMIZATION ALGORITHM

A simple algorithm was developed to find the optimum combination of C_T, λ and C_{nu} within a reasonable level of granularity. The algorithm was written in the Matlab® environment. Starting from an initial guess of the optimum operating parameters, the algorithm runs an initial simulation. Then, with λ and C_{nu} fixed, C_T is increased by an increment of 0.05 and a new simulation is run. The algorithm then chooses whether to search towards higher or lower C_T, depending on whether C_P has increased or decreased from the first simulation. Simulations are run at C_T intervals of 0.05 until the maximum C_P point is bracketed. It would be possible to use a polynomial curve fit to define the optimum C_T, however in the interest of keeping the required number of simulations to a minimum, the optimum C_T is taken as the best simulated value. C_T is then fixed, and the same strategy is used to optimize λ using increments of 1.0, and then C_{nu} using increments of 0.1. The entire process is then iterated until no change in the optimized operating parameters occurs for an entire loop.

It would be possible to run this algorithm with rather large increments to bracket the optimum design within a relatively large region of the search space. Then the chosen increments could be reduced to refine the search. The required resolution of the search space depends on the rate of change of the target variable (in this case C_P) which was found to be slow enough with the chosen increments in this case. A potential alternative to the described methodology is the golden section algorithm. Gradient based optimization is considered too complex and computationally expensive for this application since objective function gradients are not available in the CFD framework.

UNIFORMLY LOADED CASE

It has been established in texts such as Burton *et al,* (2001) that for an ideal actuator disk in open flow, uniform axial loading gives optimal performance. Shives and Crawford (2010a) showed that flow separation of the duct boundary layer is a limiting factor in the performance enhancement that can be achieved using a diffuser. Prior to completing this research it was thought that by loading the disk more heavily near the center, and more lightly near the blade tips, some flow could be diverted towards the duct surface, energizing the boundary layer and delaying flow separation. This ought to give an overall performance enhancement by allowing increased mass flow through the turbine. As a baseline case, the uniformly loaded disk was optimized by modifying the aforementioned algorithm to keep C_{nu} constant at a value of 1.0. Running this produced an optimum design where $C_T = 0.8$ and $\lambda = 4$ with a power coefficient $C_P = 0.82$. The axial flow for this simulation is shown in the top plot of Fig. 6, which shows the large region of separated flow along the downstream portion of the duct surface.

NON-UNIFORM CASE

The algorithm was run allowing C_{nu} to vary freely. The initial condition was $C_T = 0.85$, $\lambda = 4$ and $C_{nu} = 1.0$. The algorithm converged after two full loops, to $C_T = 0.80$, $\lambda = 4$, and $C_{nu} = 1.3$. This required a total of fourteen cases being examined by the algorithm. The total runtime was approximately 4 hours. As hoped, the optimum design significantly improved performance over the uniformly loaded case. The power coefficient improved from 0.82 to 0.88, an increase of 7.3%. The axial flow behavior of the optimized design is shown in the middle plot of Fig. 6.

Robustness of Design

It is important to note that the case with the best performance is very similar to that with the worst. When C_T was increased from the optimal value of 0.80 to 0.85, C_P dropped from 0.88 to 0.68. This large degradation in power was associated with a region of reversed flow just downstream of the turbine near the center of the wake, clearly shown in the bottom plot of Fig. 6. Such an abrupt change in flow behaviour is a concern for design purposes; while the determined optimum design point does maximize performance at the design condition, the off-design performance may suffer drastically. Additionally, such an unstable flow regime could lead to large fluctuations in the applied loads on the structure, leading to early failure. Interestingly, the swirl component of velocity also undergoes a dramatic shift as C_T increases to 0.90 as can be seen in Fig. 7.

Blade Characteristics

For the optimized case, the blade geometry was determined using equations 10-12, which are valid for any arbitrary airfoil with the same maximum *l/d* as used in the simulation, thus there is no requirement for specific airfoil data in defining the optimum blade geometry. The *l/d* in the present case was 40, the lift coefficient for maximum *l/d* was $c_l = 0.7$, and the corresponding angle of attack was $\alpha = 5°$. Note that wind turbines often have a lift-to-drag ratio exceeding 100, so the value of 40 used here is quite conservative. The calculated blade properties are shown in Fig. 8. The leftmost plot shows the solidity, which is defined as the length of *N* blade chords as a percentage of the circumference of a circle at a given radius. Near the blade root, the solidity is very close to 100%, meaning that the blades would be nearly overlapping. The middle plot shows the ratio of chord to turbine radius

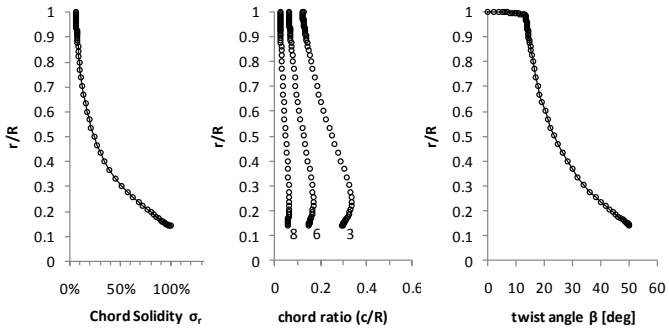

Fig. 8: Calculated blade properties for the optimum case

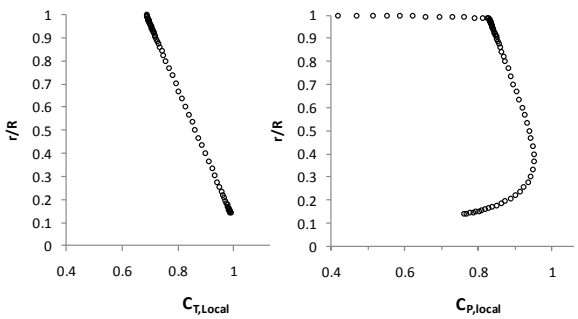

Fig. 9: Local thrust and power coefficients for the optimum case.

for designs using 3, 6 and 8 blades. Because an actuator disk approach has been used and there is no model used for discrete blade effects, the turbine performance does not depend on the number of blades. In reality, discrete blade effects will have some impact on the flow-field and turbine performance; however no model exists at present to quantify these effects for a ducted turbine. Work is ongoing to develop an actuator line approach to quantify these effects. The plot on the right of Fig. 8 shows the blade twist distribution where the inboard twist is 50° and at the tip the twist is about 13° until the duct boundary layer, where it approaches 0°. Depending on the power takeoff system, the blades may be attached to a central hub, or to an annulus housed inside the duct. Therefore, it may be possible for the blades to extend to the duct surface.

The local thrust and power coefficients were calculated using equations 15 and 16 and are shown in Fig. 9. The linear trend in C_T is evident, with more thrust at the root than the tip. There is a maximum local power coefficient of 0.95 at 37% radius. The trend of decreasing $C_{P,local}$ towards the blade tip occurs because of reduced rotor loading toward the tip, as well as increased drag due to higher relative blade velocity.

Flow Characteristics

The induction factors at the rotor plane for the optimum design are depicted in Fig. 10. The axial induction shown in the leftmost plot takes on negative values because the flow has been accelerated by the duct. As expected, the fastest axial flow (lowest axial induction) is near the blade tip because the turbine is more heavily loaded at the center. There is also region near the blade root with relatively faster axial flow, which is attributed to the pressure reduction in the centre of the wake due to swirl. The tangential induction (middle plot) behaves as expected, with the highest tangential velocity at the root and a trend towards zero at the tip. The rightmost plot shows a radial induction factor, which is defined as the radial velocity (positive outwards) normalized by the freestream velocity.

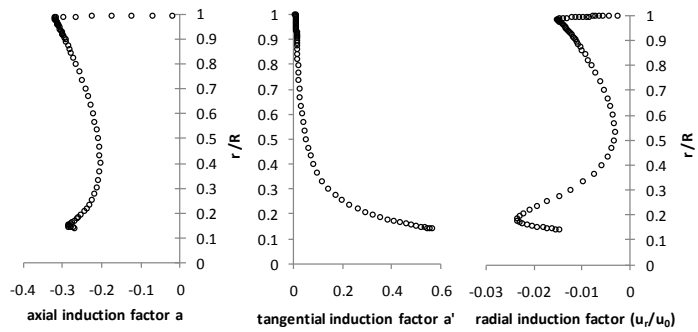

Fig. 10: Induction factors calculated for the optimum case

CONCLUSIONS

This paper presents a combined blade-element, computational fluid dynamics model for the prediction of performance and optimization of ducted turbines. With specified thrust coefficient, tip speed ratio, and non-uniformity parameter, the CFD model computed the tangential force and flowfield at the rotor plane. These parameters were then used to calculate the power coefficient and required blade geometry.

A simple algorithm was used to determine the set of input parameters (C_T, λ and C_{nu}) that maximize the power within a set level of granularity. This approach is reasonably fast, requiring approximately 15 to 30 minutes per simulation. The number of iterations until the design converges depends on how precisely the optimum parameters are to be defined. Here, the precision on C_T, λ and C_{nu} was 0.05, 1 and 0.1, respectively, and the optimization required approximately 4 hours to run using 4 parallel processes on a recent i7core PC. It is expected that more advanced techniques for bracketing the optimum will lead to less simulations being required, however the authors consider the present method fast enough for design work.

The model has revealed that it is feasible to use a non-uniform turbine loading to improve overall performance of a ducted turbine by reducing flow separation in the diffuser. Previous work by Shives and Crawford (2010a) showed that flow separation is a limiting factor in the performance enhancement possible by a duct. Using a non-uniform loading therefore may allow a large performance enhancement without the added design complexity of other boundary layer flow control devices. It remains to be seen if a non-uniform loading would improve power for a duct that does not have flow separation in the first place - this research is currently underway.

Using an actuator disk model may cause an over-estimation of the benefit of a non-uniform loading, since with discrete blades the flow could be diverted between the blades instead of radially outward. This would produce less transfer of momentum to the boundary layer and less reduction of flow separation. Discrete blade effects, commonly referred to as tip loss, are also expected to impact the flow field and turbine performance; however there is presently no model for tip loss in a duct. For these reasons, an actuator line CFD model is under development to attempt to quantify these effects.

ACKNOWLEDGMENTS

The authors thank the National Sciences and Engineering Research Council (NSERC) of Canada, the Pacific Institute for Climate Solutions (PICS) and the University of Victoria for financial support.

REFERENCES

Lilley, G. M. and Rainbird, W. J. Rep. 102: *A Preliminary Report on The Design and Performance of Ducted Windmills.* College of Aeronautics, Cranfield 1956. Available as Tech. Rep. C/T 119, The Electrical Research Association, Leatherhead, England (1957).

Foreman, K. M., Gilbert, B., and Oman, R. A., *Diffuser Augmentation of Wind Turbines*. Solar Energ, 20: pp. 305-311, 1978

Lawn, C. J., *Optimization of the power output from ducted turbines*. Proc. Instn Mech. Engrs Vol. 217 Part A: J. Power and Energy, 217: pp. 107-117, 2003

Jamieson, P., *Generalized Limits for Energy Extraction in a Linear constant Velocity Flow Field*. Wind Energy, 11: pp. 445-457, 2008. doi:10.1002/we.268

Jamieson, P. *Beating Betz: Energy Extraction Limits in a Constrained Flow Field*. Journal of Solar Energy Engineering, 131: pp. 031008-01 to 031008-06, 2009. doi:10.1115/1.3139143

Burton, T., Sharpe, D., Jenkins, N., and Bossanyi, E. *Wind Energy Handbook*. John Wiley & Sons Ltd., 2001

Hansen, M. O. L., Sorensen, N. N., and Flay, R. G. J. *Effect of Placing a Diffuser around a Wind Turbine*. Wind Energy, 3: pp. 207-213, 2000. doi:10.1002/we.37

Hansen M.O.L., Sørensen J.N., Voutsinas S., Sørensen N. and Madsen H.A, *State of the art in wind turbine aerodynamics and aeroelasticity,* Progress in Aerospace Sciences, 42:pp285-330, 2006.

Sun X.. Chick J.P, and Bryden I.G., *Laboratory-scale simulation of energy extraction from tidal currents*, Renewable Energy, 33: pp.1267-1274, 2008

Harrison M.E., Batten W.M.J., Myers L.E. and Bahaj A.S., *Comparison between CFD simulations and experiments for predicting the far wake of horizontal axis tidal turbines*, IET Renew. Power Gener., 4:pp.613-627, 2010.

Singh R. and Dinavahi S., *Shape Optimization of a Ducted Rotor System for Aerodynamic Performance*, 49th AIAA Aerospace Sciences Meeting including the New Horizons Forum and Aerospace Exposition, 4 - 7 January 2011, Orlando, Florida.

Mikkelsen, R. *Actuator Disc Methods Applied to Wind Turbines*, PhD. Thesis, University of Denmark, 2003

Réthoré, P.E., Sørensen N.N.and Zahle, F, 2010. *Validation of an Actuator Disc Model*. Wind Energy Research. http://windenergy research.org/?p=19., presented at EWEC 2010

Conway J.T., *Analytical solutions for the actuator disk with variable radial distribution of load*. J. Fluid Mech. 297:pp.327-355, 1995.

Shives, M. and Crawford, C. *Computational Analysis of Ducted Turbine Performance*. In 3rd International Conference on Ocean Energy, 6 October, Bilbao, 2010a

Shives, M. and Crawford, C. *Overall Effciency of Ducted Tidal Current Turbines*. In Proceedings of the OCEANS 2010 MTS/IEEE SEATTLE Conference & Exhibition, 2010b

Celik, I., Ghia, U., Roache, P., Freitas, C., Coleman, H., and Raad, P. *Procedure for Estimation and Reporting of Uncertainty Due to Discretization in CFD Applications*. Journal of Fluids Engineering, 130, 2008